https://doi.org/10.15407/ujpe66.4.333

V.V. ROMAKA,[1,2] YU.V. STADNYK,[3] P.F. ROGL,[4] L.P. ROMAKA,[3]
V.YA. KRAYOVSKYY,[2] A.YA. HORPENYUK,[2] A.M. HORYN[3]

[1] Leibniz Institute for Solid State and Materials Research Dresden
(Helmholtzstr., 20, Dresden 01069, Germany; e-mail: v.romaka@ifw-dresden.de)
[2] Lviv Polytechnic National University
(12, S. Bandery Str., Lviv 79013, Ukraine)
[3] Ivan Franko National University of Lviv
(Kyryla and Mephodiya Str. 6, Lviv 79005, Ukraine)
[4] University of Vienna
(Währingerstr. 42, Vienna A-1090, Austria)

MECHANISM OF DEFECT FORMATION IN $Zr_{1-x}V_xNiSn$ THERMOELECTRIC MATERIAL

Crystal and electronic structure, transport and energy state characteristics of the $Zr_{1-x}V_xNiSn$ ($0.01 \le x \le 0.1$) thermoelectric material are investigated in the 80–400 K temperature interval. A mechanism of simultaneous generation of structural defects of the acceptor and donor nature, which determines the electric conductivity of the material, is established. It is shown that energetically expedient is a simultaneous occupation of the 4c position of Ni ($3d^84s^2$) atoms by V ($3d^34s^2$) atoms, which generates structural defects of the acceptor nature and the impurity acceptor band ε_A^1, as well as the 4a position of Zr ($4d^25s^2$) atoms, generating structural defects of the donor nature and the impurity donor band ε_D^2.

Keywords: semiconductors, crystal lattices, defects.

1. Introduction

Semiconducting solid solutions based on half-Heusler ZrNiSn, TiNiSn, and HfNiSn phases are characterized by a high efficiency of the thermal to electrical energy transformation, stable properties in a wide temperature range, and high thermoelectric Q-factor (ZT), which is comparable to the best values for tellurides, clathrates, and skutterudites [1, 2].

The optimization of thermoelectric materials based on the above-mentioned compounds to obtain maximum values of the thermoelectric Q-factor depends on several factors, in particular, the concentration of charge carriers, scattering mechanisms, thermal conductivity, effects of structural disorder, *etc.* One of the ways to increase ZT values of these materials is to perform the appropriate doping with donor and/or acceptor impurities [1, 3], which change the material to a heavily doped and strongly compensated semiconductor (HDSCS) [4]. Therefore, the understanding of electrical conductivity mechanisms of semiconducting solid solutions based on half-Heusler phases is a key to the material optimization – proper choice of type and concentration of dopants [5].

Experimental studies of the ZrNiSn phase and its solid solutions have shown that it is a semiconductor with the n-type of conductivity. Currently, there are two views on the nature of donors (*a priori doping*) and the conductivity mechanisms of the ZrNiSn semiconductor. According to [6], it is caused by a disorder of the initial crystal structure of ZrNiSn (structure type MgAgAs, space group $F\bar{4}3m$ [7]) – the 4a crystallographic site is occupied by ~1 % of Ni atoms

© V.V. ROMAKA, YU.V. STADNYK, P.F. ROGL, L.P. ROMAKA, V.YA. KRAYOVSKYY, A.YA. HORPENYUK, A.M. HORYN, 2021

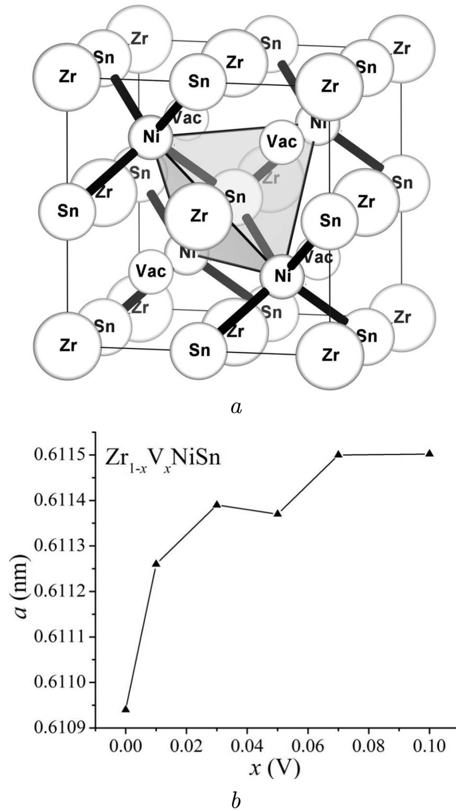

Fig. 1. Crystal structure of ZrNiSn (*a*) and concentration dependence of lattice parameters $a(x)$ (*b*) of the $Zr_{1-x}V_xNiSn$ solid solution

($3d^84s^2$) and the rest by Zr atoms ($4d^25s^2$). This type of disorder generates structural defects of the donor nature. A more recent point of view regarding the origin of donors in ZrNiSn is noteworthy. The crystal structure of ZrNiSn is characterized by the vacant 4d crystallographic site, which could be potentially filled by extra atoms (Fig. 1, *a*).

In [8], the effect of accumulation of extra Ni atoms in these voids was observed up to the $ZrNi_{1.30}Sn$ composition, which produce structural defects of the donor nature. This structural model of ZrNiSn explains the nature of its *a priori doping* by donors. In the case of full occupation of the vacant sites by extra Ni atoms, the formation of the $ZrNi_2Sn$ full-Heusler compound (structure type $MnCu_2Al$, space group $Fm\bar{3}m$) is observed [7]. Despite a strong similarity in the crystal structure of half-Heusler and full-Heusler compounds, the former have no center of symmetry, which significantly affects their physical properties.

In our paper, we report the results of investigation of the new $Zr_{1-x}V_xNiSn$ thermoelectric material obtained by the partial substitution of Zr ($4d^25s^2$) by V ($3d^34s^2$) atoms at the 4a crystallographic site of ZrNiSn, which should generate structural defects of the donor nature. Such doping satisfies the conditions [5] of achieving the maximum efficiency of thermal into electrical energy conversion in a semiconducting material. The importance of the simultaneous consideration of different mechanisms of generation of donors in the analysis of thermoelectric properties is discussed, because their contrasting or ignoring leads to the contradiction in numerous experimental studies [1, 8].

2. Experimental Details

Alloys for the investigation (2*g* each) were prepared by the conventional arc melting on a water-cooled copper hearth in the inert gas atmosphere (Ar, 5N) using appropriate amounts of ingots of Zr, V, Ni, and Sn with a purity better than 99.9%. The heat treatment was performed at 1073 K for 720 h in evacuated quartz ampoules. The samples were investigated by X-ray powder diffraction, collected from a HUBER-Gunier image plate with monochromatic $CuK_{\alpha1}$-radiation ($\lambda = 0.154056$ nm), and pure Ge (99.9999%) as internal standard. Precise lattice parameters were calculated by least squares fits to the indexed 2θ values (calibrated with respect to Ge; $a_{Ge} = 0.565791$ nm at room temperature) using the WinCSD [9] program package. The quantitative Rietveld refinement was used to determine the sites of atoms, their distribution employing the program FullProf [10]. Microstructure and chemical composition were analyzed by scanning electron microscopy (SEM) and electron probe microanalysis (EPMA) on the Zeiss SUPRA 55VP equipment with an EDX detector. Measurements of the electrical resistivity (ρ) and Seebeck (S) coefficient were carried out in the temperature interval 80–400 K and $N_D^V \approx$ $\approx 1.9 \times 10^{20}$ cm^{-3}÷1.9×10^{21} cm^{-3} ($x = 0.01$÷0.10).

The DFT calculations were carried out using the program package AkaiKKR [11, 12] employing the Korringa–Kohn–Rostocker (KKR) method with the coherent potential approximation (CPA) in the local density approximation (LDA) with the Moruzzi–Janak–Williams [13] parametrization. The energy window that covers the conduction band, semicore and valence states was equal to 21.8 eV. The ground state

energy and the distribution of the density of states (DOS) were calculated using the experimental values of lattice parameters. The Brillouin zone integration and calculation of the density of states were performed on the basis of 1000 k-points.

3. Crystal Structure of $Zr_{1-x}V_xNiSn$

According to the EPMA data, the overall composition of the annealed $Zr_{1-x}V_xNiSn$ samples is in good agreement with their nominal compositions, and no traces of impurity phases were observed. This result is confirmed by the powder XRD analysis, which showed the samples to be phase-pure. The substitution of Zr atoms ($r_{Zr} = 0.160$ nm) with smaller V atoms ($r_V = 0.134$ nm) is expected to decrease the unit cell lattice parameter. In this case, structural defects of the donor nature will be generated in the 4a crystallographic site of Zr atoms, and an impurity donor band ε_D^2 will be formed inside the band gap near the conduction band ε_C. However, the results of structural studies do not confirm this expectation. As can be seen from Fig. 1, *b*, the lattice parameters of the $Zr_{1-x}V_xNiSn$ solid solution are increasing in the concentration interval $0 \leq x \leq 0.07$. It is clear that the experimentally established behavior of the $a(x)$ dependence reflects more complex processes in the crystal structure of the solid solution than simply the Zr for V substitution in the 4a site. Unfortunately, the lack of the XRD sensitivity and small impurity concentrations do not allow us to trace, in detail, all structural changes that occur.

Several possible ways of the distribution of atoms in the $Zr_{1-x}V_xNiSn$ solid solution can be considered. The substitution of Sn (4b site) for V can be ruled out due to the larger atomic radius of Sn ($r_{Sn} = 0.162$ nm) in comparison to V. In contrast to the atomic radii of Zr and Sn, the atomic radius of Ni ($r_{Ni} = 0.124$ nm) is the smallest one, and the partial Ni for V substitution in the 4c crystallographic site may lead to increasing the lattice parameters of the $Zr_{1-x}V_xNiSn$ solid solution, which is consistent with the results of structural studies (Fig. 1, *b*). In this case, in parallel to the formation of structural defects of the donor nature, caused by the Zr for V substitution, the generation of additional structural defects of the acceptor nature (Ni for V substitution) will occur. As a result, the impurity acceptor band ε_A^2 near the valence band ε_V is formed.

Thus, the performed structural studies of the $Zr_{1-x}V_xNiSn$ solid solution do not allow us to consistently explain the mechanisms of distribution of atoms, which leads to unpredictable changes in the electronic structure and kinetic properties of a thermoelectric material.

4. Band Structure of Ordered $Zr_{1-x}V_xNiSn$

To predict the behavior of the Fermi level ε_F, the band gap ε_g, the kinetic characteristics of $Zr_{1-x}V_xNiSn$, the electronic band structure, and the distribution of the density of states (DOS) were calculated (Fig. 2) for an ordered variant of the crystal structure in which Zr atoms are replaced exclusively by V using experimentally derived lattice parameters. The Fermi level ε_F of ZrNiSn is located in the donor band ε_D^1 near the percolation level of the conduction band ε_C formed as a result of the *a priori doping*. Since the replacement of Zr atoms with V generates structural defects of the donor nature, the impurity donor zone ε_D^2 is formed at the lowest concentrations of V in $Zr_{1-x}V_xNiSn$. This will increase the concentration of donors, and the Fermi level ε_F will approach the percolation level of the conduction band ε_C, which will increase the density of states at the Fermi level $g(\varepsilon_F)$. The drift of the Fermi level into the conduction band will change the electrical conductivity type from activation to metallic one [4]: the activation region on the $\ln(\rho(1/T))$ dependences will disappear, and the resistivity will increase with the temperature and V concentration. However, the density of states at the Fermi level $g(\varepsilon_F)$ increases much slower.

5. Transport and Energetic Properties of $Zr_{1-x}V_xNiSn$

The temperature and concentration dependences of the resistivity ρ and the Seebeck coefficient S of $Zr_{1-x}V_xNiSn$ are shown in Figs. 3, 4. The dependences of $\ln(\rho(1/T))$ and $S(1/\mathrm{T})$ presented in Fig. 3 are typical of HDSCS, and the activation regions indicate several mechanisms of charge transfer. The $\ln(\rho(1/T))$ dependence is described by the following relation [4]:

$$\rho^{-1}(T) = \rho_1^{-1} \exp\left(-\frac{\varepsilon_1^\rho}{k_B T}\right) + \rho_3^{-1} \exp\left(-\frac{\varepsilon_3^\rho}{k_B T}\right), \quad (1)$$

where the first high-temperature term describes the activation of charge carriers ε_1^ρ from the Fermi level ε_F

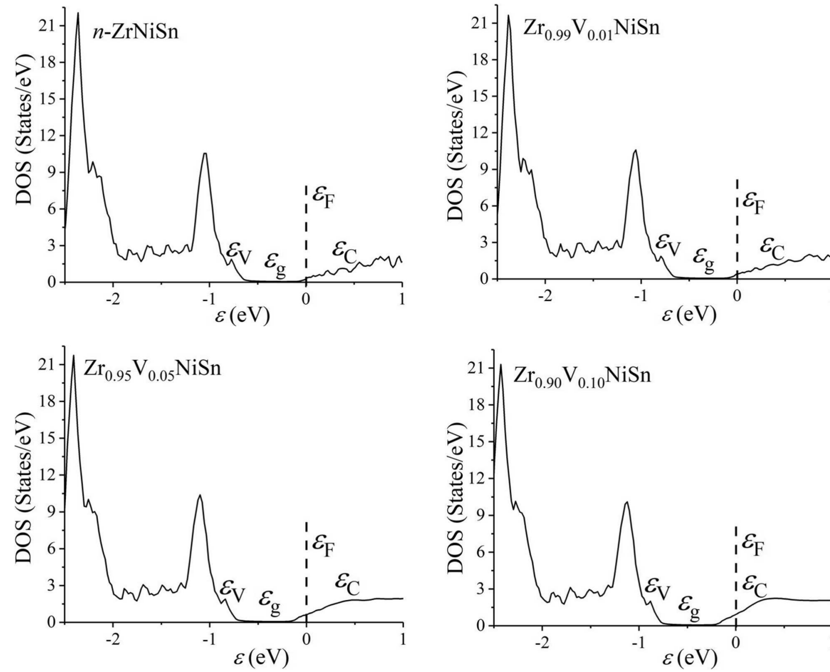

Fig. 2. Distribution of the density of states for the ordered model of the crystal structure of ZrNiSn, $Zr_{0.99}V_{0.01}NiSn$, $Zr_{0.95}V_{0.05}NiSn$, and $Zr_{0.90}V_{0.10}NiSn$

onto the percolation level of the conduction/valence band. The second low-temperature term describes the hopping conductivity ε_3^ρ.

The temperature dependences $S(1/T)$ are approximated by the following expression [14]:

$$S = \frac{k_\mathrm{B}}{e}\left(\frac{\varepsilon_i^S}{k_\mathrm{B}T} - \gamma + 1\right), \tag{2}$$

where γ is a parameter that depends on the scattering mechanisms. The ε_1^S and ε_3^S activation energies are calculated from the high- and low-temperature regions of the $S(1/T)$ dependences, respectively. The ε_1^S activation energy is proportional to the amplitude of a large-scale fluctuation of the conduction/valence band, while the ε_3^S is proportional to the amplitude of a small-scale fluctuation of the conduction/valence band of HDSCS [1, 4].

For ZrNiSn, the activation energies ε_1^ρ and ε_3^ρ, derived from the $\ln(\rho(1/T))$ dependence, are equal to 97.6 and 11.9 meV, respectively, while those derived from the $S(1/T)$ dependence are $\varepsilon_1^S = 83.8$ meV and $\varepsilon_3^S = = 11.5$ meV.

The doping of the half-Heusler ZrNiSn compound with V atoms changes the behavior of the temperature and concentration dependences of the resistivity $\rho(x,T)$ and the Seebeck coefficient $S(x,T)$ (Figs. 3, 4). From DOS calculations, we predicted that the substitution of Zr atoms by V in $Zr_{1-x}V_xNiSn$ would generate structural defects of the donor nature, which corresponds to the negative values of the Seebeck coefficient $S(x,T)$. Indeed, as can be seen from Figs. 3 and 4, *b*, the Seebeck coefficient at all concentrations and temperatures remains negative. The generation of additional donors increases the concentration of free electrons decreasing the resistivity $\rho(x,T)$. Such behavior of $\rho(x,T)$ can be seen in Figs. 3 and 4, *a*.

The high-temperature activation regions on the $\ln(\rho(1/T))$ dependences are observed in all $Zr_{1-x}V_xNiSn$ samples (Fig. 3). Their presence indicates the location of the Fermi level ε_F in the band gap of the semiconductor material. The negative values of the Seebeck coefficient $S(x,T)$ indicate that the Fermi level is in the band gap near the conduction band. This fact is inconsistent with the results of band structure calculations of $Zr_{1-x}V_xNiSn$ for an ordered model of the crystal structure in which the substitution of Zr for V atoms occurs at the 4a site, generating structural defects of the donor nature. According to the modeling (Fig. 2), the Fermi level enters the conduction band

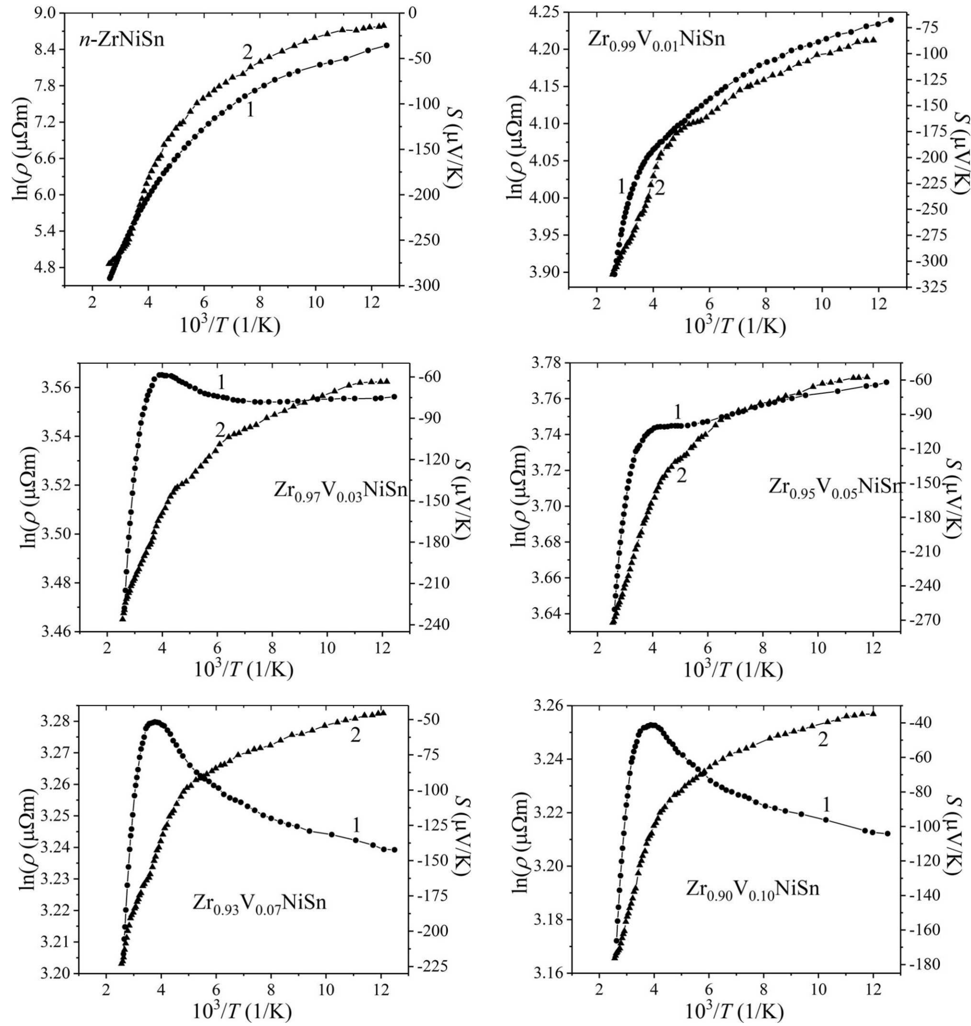

Fig. 3. Temperature dependences of the electrical resistivity $\ln(\rho(1/T))$ (curve *1*) and the Seebeck coefficient $S(1/T)$ (curve *2*) of ZrNiSn, $Zr_{0.99}V_{0.01}NiSn$, $Zr_{0.97}V_{0.03}NiSn$, $Zr_{0.95}V_{0.05}NiSn$, $Zr_{0.93}V_{0.07}NiSn$, and $Zr_{0.90}V_{0.10}NiSn$

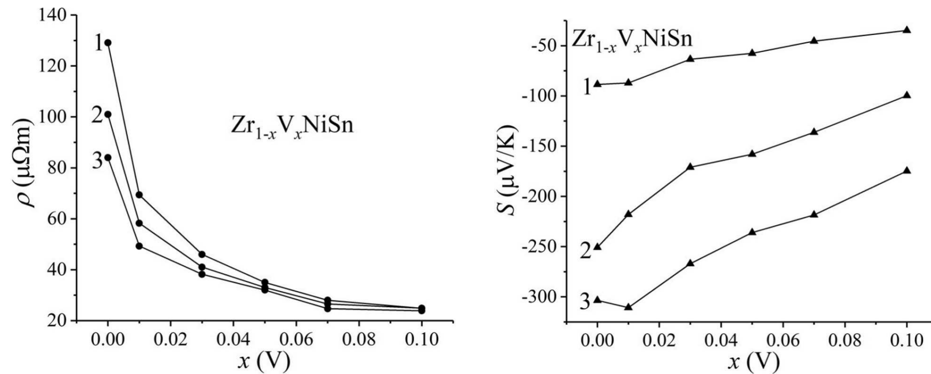

Fig. 4. Temperature dependences of the electrical resistivity $\rho(x,T)$ (*a*) and the Seebeck coefficient $S(x,T)$ (*b*) at *1* – 80 K, *2* – 250 K, *3* – 380 K of the $Zr_{1-x}V_xNiSn$ solid solution

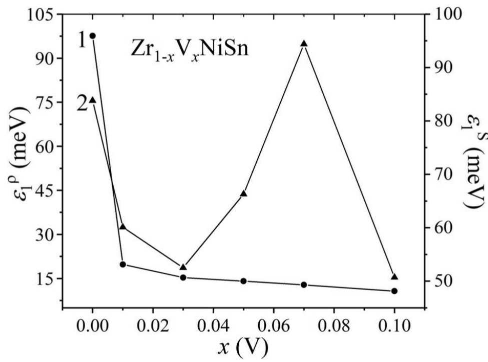

Fig. 5. Concentration dependences of the ε_1^ρ (*1*) and ε_1^S (*2*) activation energies of the $Zr_{1-x}V_xNiSn$ solid solution

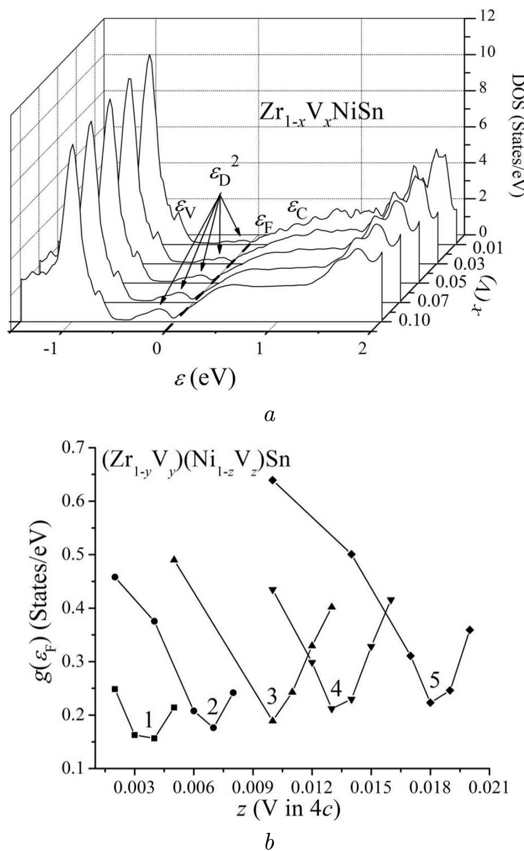

Fig. 6. Distributions of the total density of states (*a*) and the density of states at the Fermi level (curves *1, 2, 3, 4*, and *5* correspond to $x = 0.01$, 0.03, 0.05, 0.07, and 0.10, respectively) (*b*) for the disordered model of the $Zr_{1-x}V_xNiSn$ solid solution

already at $x \geq 0.01$ that leads to the metallic type of conductivity.

Thus, the presence of the high-temperature activation region at all concentrations of V evidences the formation of structural defects of the acceptor nature. These acceptors capture the free electrons, reducing their concentration, and slow down the drift of the Fermi level toward the conduction band. Using the experimental value of the $\varepsilon_1^\rho(x)$, we can identify the character of the drift of the Fermi level in the energy gap. The distance from the Fermi level to the conduction band $\varepsilon_1^\rho(x)$ changes from 97.6 meV in ZrNiSn to 19.8 meV in $Zr_{0.99}V_{0.01}NiSn$ (Fig. 5). For higher V concentrations, the drifting speed of the Fermi level significantly decreases. In $Zr_{0.97}V_{0.03}NiSn$, the Fermi level is at the distance of $\varepsilon_1^\rho = 15.3$ meV from the conduction band. However, higher V concentrations only slightly decrease this distance: $\varepsilon_1^\rho(x = 0.05) = 14.1$ meV, $\varepsilon_1^\rho(x = 0.10) = 10.7$ meV. The number of V atoms introduced into the crystal structure of ZrNiSn linearly increases and should, in theory, linearly increase the number of generated donor defects and the drifting speed of the Fermi level toward the conduction band. However, even with a significant concentration of the donor impurity, $N_D^V \approx 1.9 \times 10^{21}$ cm^{-3} ($x = 0.10$), the Fermi level remains inside the band gap. The reason for this is the simultaneous generation of donors and acceptors. The latter capture free electrons and change a compensation degree of the semiconductor. The ε_1^S activation energy, derived from the $S(1/\mathrm{T})$ dependence (Fig. 3), which reflects the compensation degree of $Zr_{1-x}V_xNiSn$ and changes the degree of compensation of the semiconductor, decreases from 83.8 meV for $x = 0$ to 60.1 meV ($x = 0.01$) and 52.5 meV ($x = 0.03$). Such a decrease in the activation energy indicates that donors are predominantly generated. The generation of acceptors is also possible, but the number of ionized donors far exceeds the number of acceptors. At higher V concentrations, the values of $\varepsilon_1^S(x)$ are also increasing, reaching the maximum at $x = 0.07$. This behavior clearly indicates that acceptors are generated at a higher rate than donors in the $Zr_{1-x}V_xNiSn$ semiconductor. This experimental result contradicts the theoretical band structure for the ordered model of the crystal structure of $Zr_{1-x}V_xNiSn$.

6. Optimization of the Crystal and Band Structures of $Zr_{1-x}V_xNiSn$

The model of the ordered crystal structure of the $Zr_{1-x}V_xNiSn$ solid solution, where Zr atoms are partially substituted by V at the 4a crystallographic site,

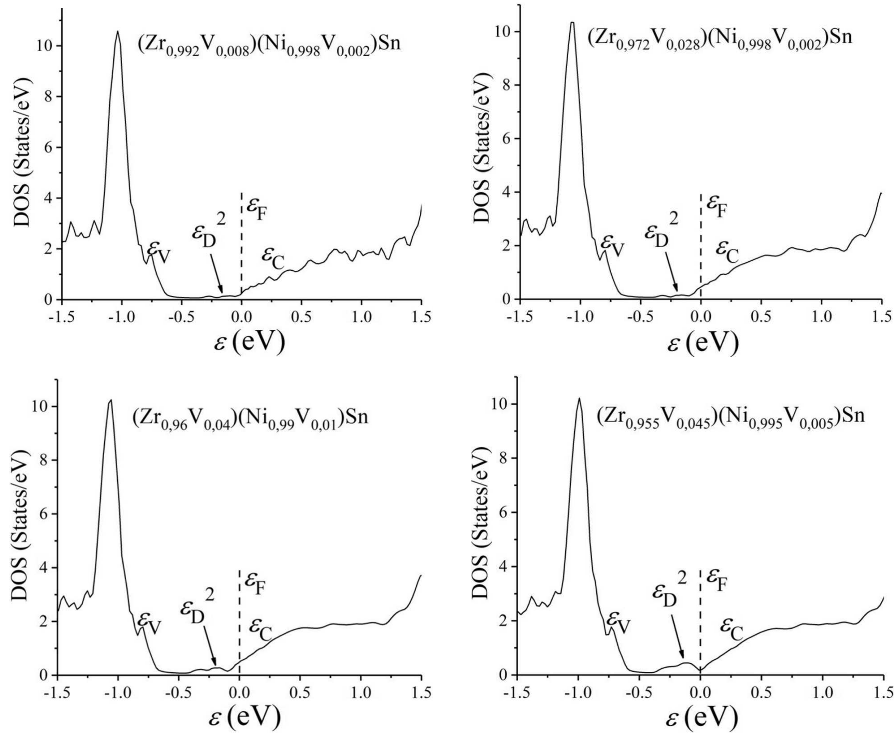

Fig. 7. Distribution of the total density of states for the disordered model of the crystal structure of $(Zr_{1-y}V_y)(Ni_{1-z}V_z)Sn$

does not explain the change in the lattice parameters, and the distribution of the density of states calculated within this model contradicts the transport properties of the material. To overcome this problem, we determined the model of the disordered crystal structure using the approach described in [1, 15], which is based on the iterative optimization of the crystal structure (anti-site disorder, vacancies at various crystallographic sites) with further band structure calculations to fit theoretical energetical parameters (activation energies, location of the Fermi level, Seebeck coefficient, *etc.*) with available experimental data.

The model of the disordered crystal structure that was used is based on the possible partial occupancy of the 4c site (originally occupied by Ni atoms) with the statistical mixture of Ni and V atoms in addition to the Zr for V substitution. The calculated total DOS distribution for this model of the $Zr_{1-x}V_xNiSn$ solid solution is presented in Fig. 6, *a*. The more detailed DOS plot (Fig. 7) shows the formation of the large donor band ε_D^2 in the band gap, which expands with increasing the V concentration. For this, we performed the band structure modeling for different Zr/V and Ni/V ratios at the 4a and 4c sites, respectively, keeping the total amount of V atoms equal to their nominal content – $(Zr_{1-y}V_y)(Ni_{1-z}V_z)Sn$. By increasing the V concentration at one site for a certain value, we decrease their amount at another site for the same value ($x = y + z$), which correspondz to different donor/acceptor ratios in the crystal and defines the location of the Fermi level in the band gap. Depending on the V content at the 4c Ni site, the density of states at the Fermi level $g(\varepsilon_F)$ significantly changes (Fig. 6, *b*). For $x = 0.01$, the $g(\varepsilon_F)$ dependence has a minimum at $z(V) \approx 0.004$ (Fig. 6, *b*, curve *1*), while, for $x = 0.10$, the $g(\varepsilon_F)$ minimum uccurs at $z(V) \approx 0.018$ (Fig. 6, *b*, curve *5*).

The simultaneous generation of donors and acceptors in different ratios will change the degree of compensation of $Zr_{1-x}V_xNiSn$, which will change the position of the Fermi level ε_F, as well as the value of the state density at the Fermi level $g(\varepsilon_F)$. The values of $g(\varepsilon_F)$ will be smallest, if the number of generated acceptors (V at the 4c site) change the degree of compensation in such a way that the Fermi

level is located in the band gap between the percolation level of the conduction band and the states of the donor band ε_D^2 (Fig. 6, *b*). With the higher total concentration of V atoms, the minimum on the $g(\varepsilon_F)$ dependence will occur at higher acceptor concentrations (V at the 4c site). The DOS modeling of disordered $(Zr_{1-y}V_y)(Ni_{1-z}V_z)Sn$ was performed for those concentrations of V atoms at the 4c site, where the minimum on the $g(\varepsilon_F)$ occurs (Fig. 6, *b*).

7. Conclusions

Thus, as a result of the complex study of the $Zr_{1-x}V_xNiSn$ thermoelectric material, a mechanism for simultaneous generation of structural defects of acceptor and donor nature is established. It is shown that energetically expedient is the simultaneous occupation of the 4c crystallographic site of Ni ($3d^84s^2$) by V ($3d^34s^2$) atoms, which generates structural defects of the acceptor nature, as well as V atoms at the 4a site of Zr ($4d^25s^2$), which is a source of structural defects of the donor nature. Inside the band gap of the $Zr_{1-x}V_xNiSn$ semiconductor, both donor ε_D^2 and acceptor ε_A^1 bands appear simultaneously, which defines the mechanisms of electrical conductivity.

The research reported herein was supported by the Ministry of Education and Science of Ukraine (Grant 0118U003609), Austrian agency for international mobility and cooperation in education, science and research (Ernst Mach project ICM-2017-06580), and German Federal Ministry of Education and Research (UKRATOP Project, 01DK18002).

1. V.A. Romaka, V.V. Romaka, Yu.V. Stadnyk. *Intermetallic Semiconductors: Properties and Applications* (Lvivska Polytechnika, 2011) [ISBN: 978-617-607-053-5] (in Ukrainian).
2. V.V. Romaka, P.-F. Rogl, R. Carlini, C. Fanciulli. Prediction of the thermoelectric properties of half-heusler phases from the density functional theory. In: *Alloys and Intermetallic Compounds.* Ed. by C. Artini (Taylor and Francis Group, 2017) [ISBN: 978-1-4987-4143-9].
3. L.I. Anatychuk. *Thermoelements and Thermoelectric Devices* (Naukova Dumka, 1979).
4. B.I. Shklovsky, A.L. Efros. *Electronic Properties of Doped Semiconductors* (Springer, 1984).
5. V.A. Romaka, D. Fruchart, Yu.V. Stadnyk, J. Tobola, Yu.K. Gorelenko, M.G. Shelyapina, L.P. Romaka, V.F. Chekurin. Conditions for attaining the maximum values of thermoelectric power in intermetallic semiconductors of the MgAgAs structural type. *Semiconductors* **40**, 1275 (2006).
6. D. Fruchart, V.A. Romaka, Yu.V. Stadnyk, L.P. Romaka, Yu.K. Gorelenko, M.G. Shelyapina, V.F. Chekurin. Conductivity mechanisms in heavy-doped n-ZrNiSn intermetallic semiconductors. *J. Alloys Compd.* **438**, 8 (2007).
7. V.V. Romaka, L.P. Romaka, V.Ya. Krayovskyy, Yu.V. Stadnyk. *Stannides of Rare Earths and Transition Metals* (Lvivska Polytechnika, 2015) [ISBN: 978-617-607-816-6] (in Ukrainian).
8. V.A. Romaka, P.-F. Rogl, V.V. Romaka, Yu.V. Stadnyk, E.K. Hlil, V.Ya. Krayovskyy, A.M. Goryn. Effect of the accumulation of excess Ni atoms in the crystal structure of the intermetallic semiconductor *n*-ZrNiSn. *Semiconductors* **47**, 892 (2013).
9. L. Akselrud, Yu. Grin. WinCSD: Software package for crystallographic calculations (Version 4). *J. Appl. Crystallogr.* **47**, 803 (2014).
10. T. Roisnel, J. Rodriguez-Carvajal. WinPLOTR: A Windows tool for powder diffraction patterns analysis. *Mater. Sci. Forum* **378–381**, 118 (2001).
11. H. Akai. Fast Korringa–Kohn–Rostoker coherent potential approximation and its application to fcc Ni–Fe systems. *J. Phys.: Condens. Matter* **1**, 8045 (1989).
12. M. Schruter, H. Ebert, H. Akai, P. Entel, E. Hoffmann, G.G. Reddy. First-principles investigations of atomic disorder effects on magnetic and structural instabilities in transition-metal alloys. *Phys. Rev. B* **52**, 188 (1995).
13. V.L. Moruzzi, J.F. Janak, A.R. Williams. *Calculated Electronic Properties of Metals* (Pergamon Press, 1978).
14. N.F. Mott, E.A. Davis. *Electron Processes in Non-Crystalline Materials* (Clarendon Press, 1979).
15. V.V. Romaka, G. Rogl, A. Grytsiv, P. Rogl. Determination of structural disorder in Heusler-type phases. *Comp. Mater. Sci.* **172**, 109307 (2020).

Received 25.02.2020

В.В. Ромака, Ю.В. Стадник,
П.Ф. Рогль, Л.П. Ромака, В.Я. Крайовський,
А.Я. Горпенюк, А.М. Горинь

МЕХАНІЗМ УТВОРЕННЯ ДЕФЕКТІВ
У ТЕРМОЕЛЕКТРИЧНОМУ МАТЕРІАЛІ $Zr_{1-x}V_xNiSn$

Досліджено кристалічну та електронну структуру, транспортні та енергетичні характеристики термоелектричного матеріалу $Zr_{1-x}V_xNiSn$ ($0{,}01 \leq x \leq 0{,}1$) в інтервалі температур 80–400 K. Встановлено механізми генерування структурних дефектів акцепторної та донорної природи, які визначають електропровідність матеріалу. Показано, що енергетично вигідним є одночасне заповнення як кристалографічної позиції 4c атомів Ni($3d^84s^2$) атомами V($3d^34s^2$), які генерують структурні дефекти акцепторної природи та створюють домішкову акцепторну зону ε_A^1, так і позиції 4a атомів Zr ($4d^25s^2$), які генерують структурні дефекти донорної природи та створюють домішкову донорну зону ε_D^2.

Ключові слова: напівпровідники, кристалічні ґратки, дефекти.